nature microbiology

SUPPLEMENTARY INFORMATION

DOI: 10.1038/s41564-017-0018-1

In the format provided by the authors and unedited.

Efficient invasion by *Toxoplasma* depends on the subversion of host protein networks

Amandine Guérin[1], Rosa Milagros Corrales[1], Michele L. Parker[2], Mauld H. Lamarque[1], Damien Jacot[3], Hiba El Hajj[4], Dominique Soldati-Favre[3], Martin J. Boulanger[2] and Maryse Lebrun[1]*

[1]Unité Mixte de Recherche 5235, Centre National de la Recherche Scientifique, Université de Montpellier 2, 34095 Montpellier, France. [2]Department of Biochemistry and Microbiology, University of Victoria, Victoria, BC V8P 5C2, Canada. [3]Department of Microbiology and Molecular Medicine, Centre Médical Universitaire, University of Geneva, 1 Rue Michel-Servet, 1206 Geneva, Switzerland. [4]Department of Internal Medicine and Experimental Pathology, Immunology and Microbiology, American University of Beirut, Beirut 1107 2020, Lebanon. *e-mail: mylebrun@univ-montp2.fr

Supplementary Figures and tables

Supplementary Figure 1 | YPNL and Px[P/A]xPR motifs of *Tg*RON4 are competent to bind ALIX Bro-V and CIN85-SH3ABC, respectively.

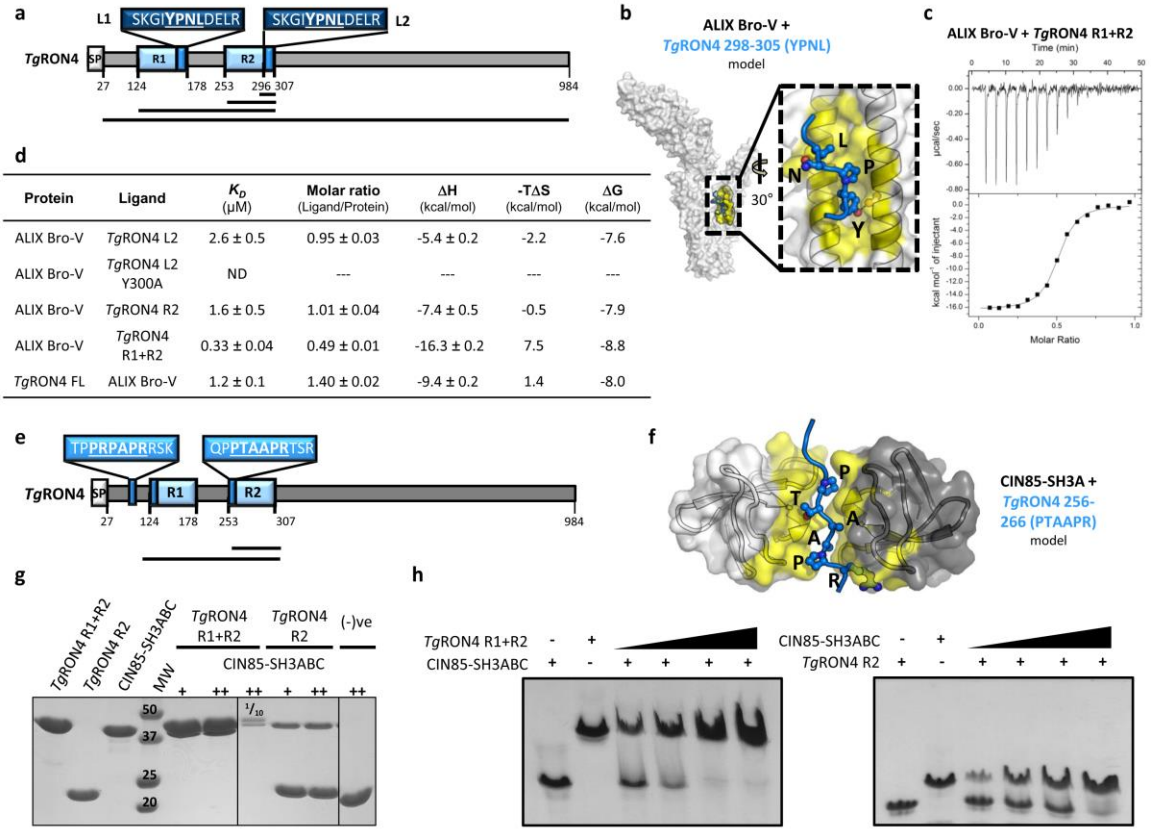

Protein	Ligand	K_D (µM)	Molar ratio (Ligand/Protein)	ΔH (kcal/mol)	-TΔS (kcal/mol)	ΔG (kcal/mol)
ALIX Bro-V	*Tg*RON4 L2	2.6 ± 0.5	0.95 ± 0.03	-5.4 ± 0.2	-2.2	-7.6
ALIX Bro-V	*Tg*RON4 L2 Y300A	ND	---	---	---	---
ALIX Bro-V	*Tg*RON4 R2	1.6 ± 0.5	1.01 ± 0.04	-7.4 ± 0.5	-0.5	-7.9
ALIX Bro-V	*Tg*RON4 R1+R2	0.33 ± 0.04	0.49 ± 0.01	-16.3 ± 0.2	7.5	-8.8
*Tg*RON4 FL	ALIX Bro-V	1.2 ± 0.1	1.40 ± 0.02	-9.4 ± 0.2	1.4	-8.0

a, Schematic of the RON4 protein sequence, with the two N-terminal repeats (R1 and R2) indicated by light blue boxes, and the Late domains (L1 and L2) containing the YPNL motifs highlighted in dark blue boxes. The black bars indicate constructs used to investigate binding of RON4 to ALIX Bro-V. SP, signal peptide. **b,** Energy minimized model of the complex between ALIX Bro-V (semi-transparent white surface) and the central portion of RON4 L2 (residues 298 to 305; blue cartoon with YPNL motif shown in ball-and-stick colored by element), with the interacting residues of ALIX Bro-V shown as a solid yellow

surface. Inset – Thirty-degree rotation showing the Tyr of the YPNL motif buried in a deep pocket and hydrogen bonding to an Asp (yellow ball-and-sticks) of ALIX Bro-V. **c,** Sample ITC thermogram of ALIX Bro-V interacting with RON4 R1+R2 TRX at 25 °C. **d,** Table of ITC results comparing binding affinities and thermodynamic profiles for the interaction of ALIX Bro-V with various fragments of RON4 at 25 °C. Protein, sample in the ITC cell; Ligand, sample in syringe. RON4 can bind to ALIX molecules. **e,** Schematic of the RON4 protein sequence, with the three N-terminal repeats of the Px[P/A]xPR motif highlighted in blue boxes. The black bars indicate constructs used to investigate binding of RON4 to CIN85-SH3ABC. **f,** Energy minimized model of the complex between CIN85-SH3A dimer (semi-transparent white and dark grey surfaces) and the N-terminal region of RON4 R2 (residues 256 to 266; blue cartoon with the PTAAPR motif shown in ball-and-stick colored by element; with the interacting residues of CIN85-SH3A colored yellow. **g,** SDS-PAGE of nickel affinity pull downs showing that CIN85-SH3ABC is efficiently pulled down by TRX fusions of both RON4 R1+R2 and R2, but not a negative control protein ((-)ve). Lanes to the left of the molecular weight marker (MW, kDa) are input protein, while lanes to the right are elution. **h,** Native gels of CIN85-SH3ABC interacting with RON4 R1+R2 (left) and RON4 R2 (right). Left – Dose-dependent co-migration of CIN85-SH3ABC with increasing concentrations of RON4 R1+R2. Right – Dose-dependent co-migration of RON4 R2 with increasing concentrations of CIN85-SH3ABC.

Supplementary Figure 2 │ CD2AP is recruited at the MJ via Px[P/A]xPR motifs present on RON2, RON5 and RON4.

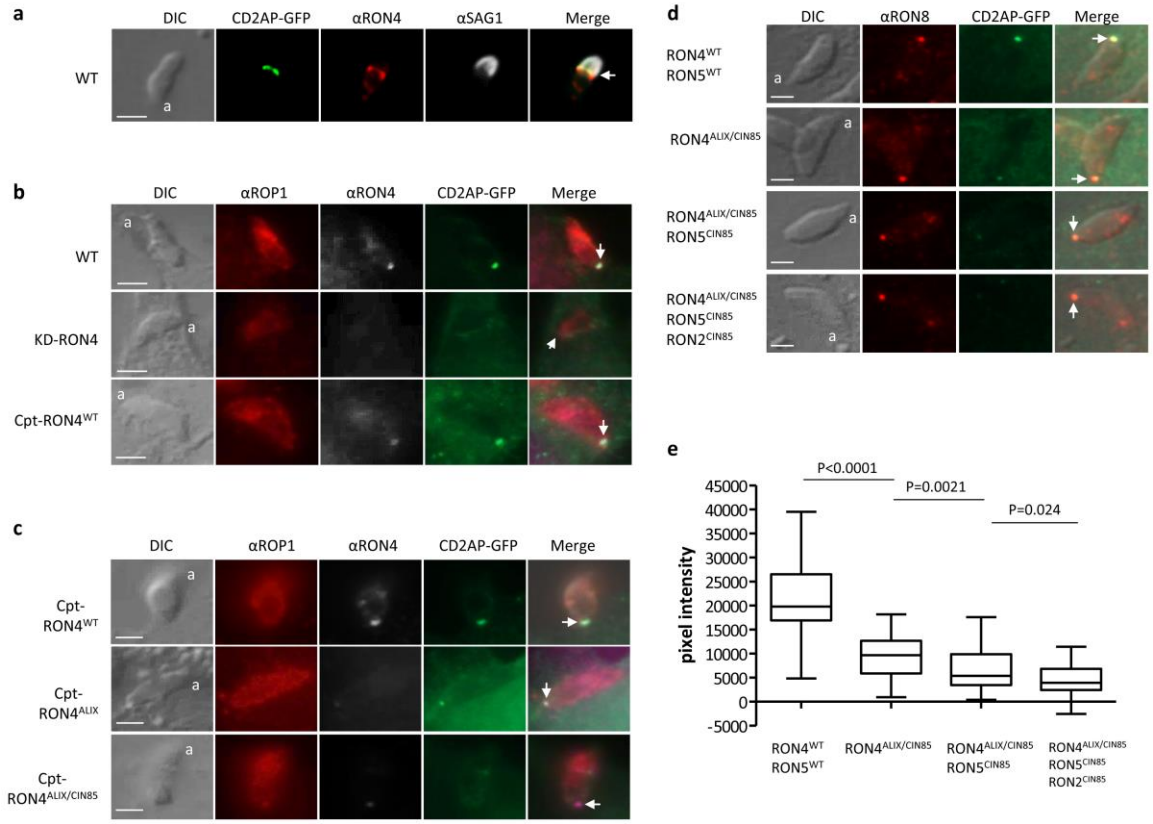

a, IFAs of invading wild-type (Δ*ku80 TATi*) parasites on HeLa cells transfected with vector allowing expression of CD2AP-GFP. CD2AP accumulates with RON4 at the MJ. Anti-RON4 antibody in red, CD2AP in green. SAG1 in white stains the extracellular part of the invading parasite. a, apical end; arrow, MJ. Scale bar, 2µm. **b,** IFAs of invading wild-type (Δ*ku80 TATi*), KD-RON4 and Cpt-RON4^{WT} on HeLa cells expressing CD2AP-GFP. CD2AP localizes at the MJ only when the RON2/RON4/RON5 complex is detectable at the MJ. Red, ROP1; White, RON4; Green, CD2AP. a, apical end; arrow, MJ. Scale bar, 2µm. **c,** IFAs of invading Cpt-RON4^{WT}, Cpt-RON4^{ALIX} and Cpt-RON4$^{ALIX/CIN85}$ parasites in HeLa cells expressing CD2AP-GFP. Red, anti-ROP1 antibodies. White, anti-RON4

antibodies. a, apical end; arrow, MJ. Scale bar 2µm. **d,** IFAs of invading parasites on HeLa cells expressing CD2AP-GFP. Red, RON8; Green CD2AP-GFP. Same exposure time for each strain. a, apical end; arrow, MJ. Scale bar, 2µm. **e,** Quantification of CD2AP recruitment at the MJ. Values represent means ± SD, n=41, from a representative experiment out of 2 independent assays. Statistical significance was calculated using a Mann-Whitney's t test.

Supplementary Figure 3 | Generation of a RON4 knock-down and complemented strains.

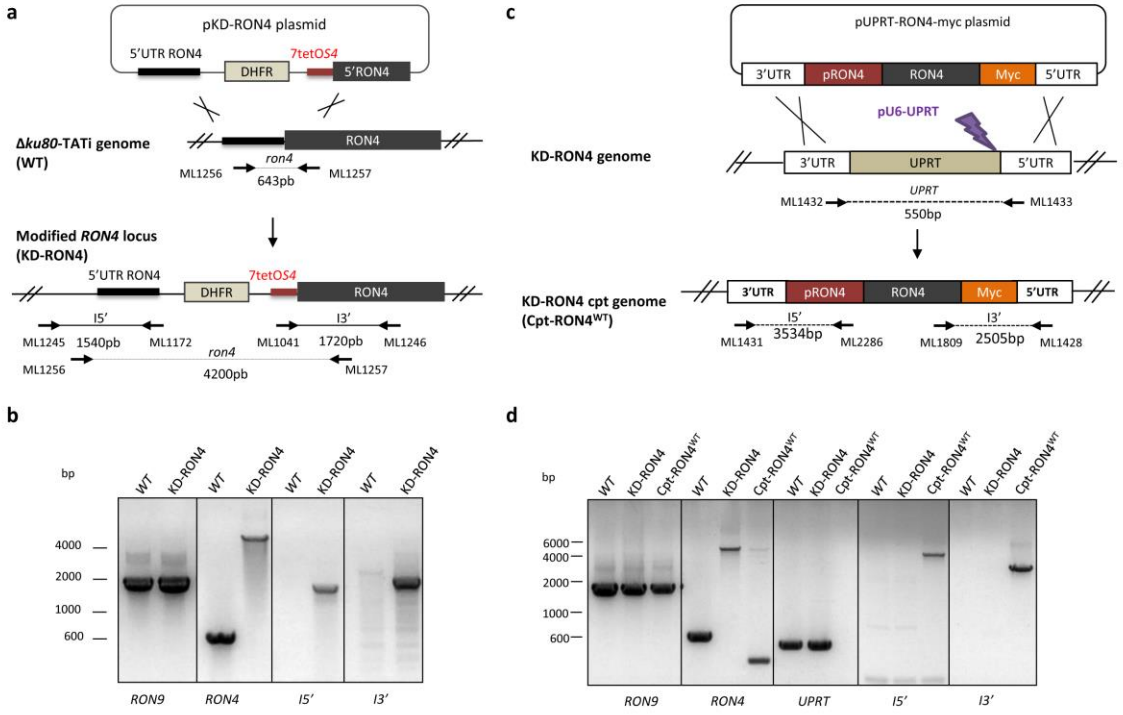

a, Schematic illustrating the approach used to generate a conditional knock-down of the *RON4* gene, KD-RON4. The endogenous promoter of RON4 was replaced by double homologous recombination with an anhydrotetracycline (ATc)-repressible promoter in the *Δku80* cell line expressing the trans-activator TATi (*Δku80-TATi*). Primers used to verify the correct integration by PCR are indicated by arrows. The expected sizes of the amplicons are also shown. **b,** The recombination at the *RON4* locus was verified with PCRs *RON4*, *I5'*and *I3'*. *RON9*: control PCR. It should be noted that the primers used to amplify the RON4 PCR product in the KD-RON4 strain allows the amplification of a 4200 bp fragment versus 634 bp in the WT strain. **c,** Schematic representing the approach used to complement KD-RON4 at the *UPRT* locus with a wild-type copy of RON4 (Cpt-RON4^{WT}). A linear pUPRT-RON4-myc plasmid containing RON4 cDNA flanked by *UPRT* sequences was

co-transfected with pU6-UPRT plasmid, targeting Cas9 to cut the *UPRT* gene. Primers used to verify the correct integration by PCR are indicated by arrows. The expected sizes of the amplicons are also shown. **d,** Integration at the *UPRT* locus was verified with PCRs *RON4* (same as described in A), *UPRT*, *I5'*, *I3'*. *RON9*: control PCR.

Supplementary Figure 4 | KD-RON4 parasites present an invasion defect due to destabilization of RON2, RON4 and RON5

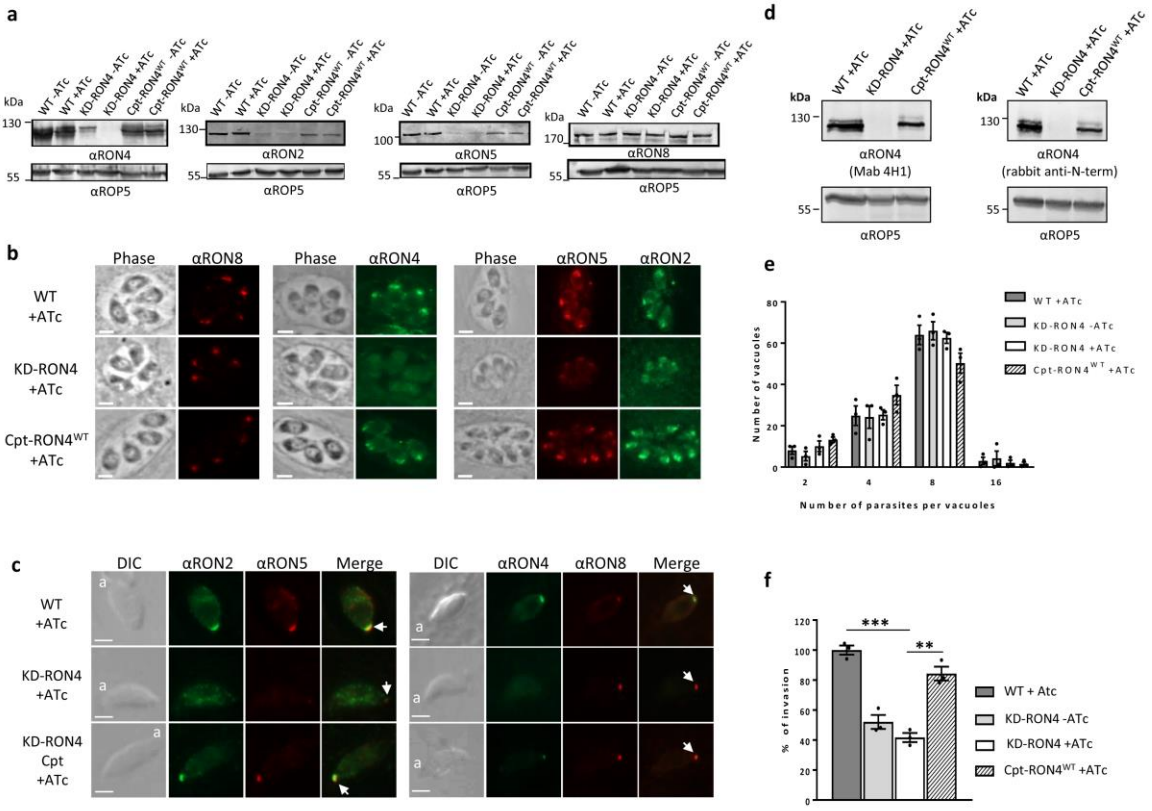

a, Immunoblot of wild-type (WT), KD-RON4 and Cpt-RON4^{WT} parasites, treated or not with 1 µM ATc for 2 days, using rabbit anti-RON4, rabbit anti-RON2-3, rat anti-RON8 and rat anti-RON5N antibodies. ROP5, loading control. Expression levels of RON4, RON2 and RON5 are decreased in KD-RON4 even in absence of ATc and partially restored in Cpt-RON4^{WT} strain. RON8 remains unchanged in KD-RON4. **b,** IFAs of intracellular WT, KD-RON4 and Cpt-RON4^{WT} parasites treated with ATc for 2 days, using mouse anti-RON4, rabbit anti-RON2-4, rat anti-RON8 and rat anti-RON5N antibodies. RON2, RON4 and RON5 signals in the rhoptry neck are either absent or lower compared to WT, while RON8 signal was not affected. Scale bars, 5 µm. Images were recorded with the same

exposure time. **c,** IFAs of invading WT, KD-RON4 and Cpt-RON4^{WT} parasites using rabbit anti-RON4, rabbit anti-RON2-4, rat anti-RON8 and rat anti-RON5N antibodies. Before invasion, parasites were grown with ATc for two days. RON4 is not detectable at the MJ of invading KD-RON4 parasites while RON2 and RON5 signals are fainter or almost undetectable compared to WT. a, apical end; arrow, MJ. Scale bars, 2 µm. All the images were recorded with the same exposure time. **d,** Immunoblots of WT, KD-RON4 and Cpt-RON4^{WT} parasites treated with ATc for two days, using anti-RON4 monoclonal antibody Mab 4H1 or a rabbit polyclonal anti-RON4 against RON4 N-term part. Densitometric quantifications of signals indicate 55% and 57% less proteins in the complemented strain versus WT using Mab 4H1 and anti-N term anti-RON4 antibodies, respectively. **e,** Replication assay for 24 hours in HFF cells of WT, KD-RON4 or Cpt-RON4^{WT}, treated or not with ATc for two days. No defect on intracellular growth is observed in the KD-RON4 mutant. Student's t test p=ns; mean ± s.e.m (n=3), from a representative experiment out of 3 independent assays. **f,** Invasion assay for 5 minutes in HFF cells of WT, KD-RON4 and Cpt-RON4^{WT} parasites. KD-RON4 parasites impaired in RON2, RON4 and RON5 expression show a significant invasion defect that is mostly restored in Cpt-RON4^{WT}. Student's t test ***$p < 0.001$, **$p < 0.01$; mean ± s.e.m (n=3), from a representative experiment out of 3 independent assays.

Supplementary Figure 5 | Mutations of ALIX and CIN85 binding sites in RON4 complemented strain do not affect RON expression and localization

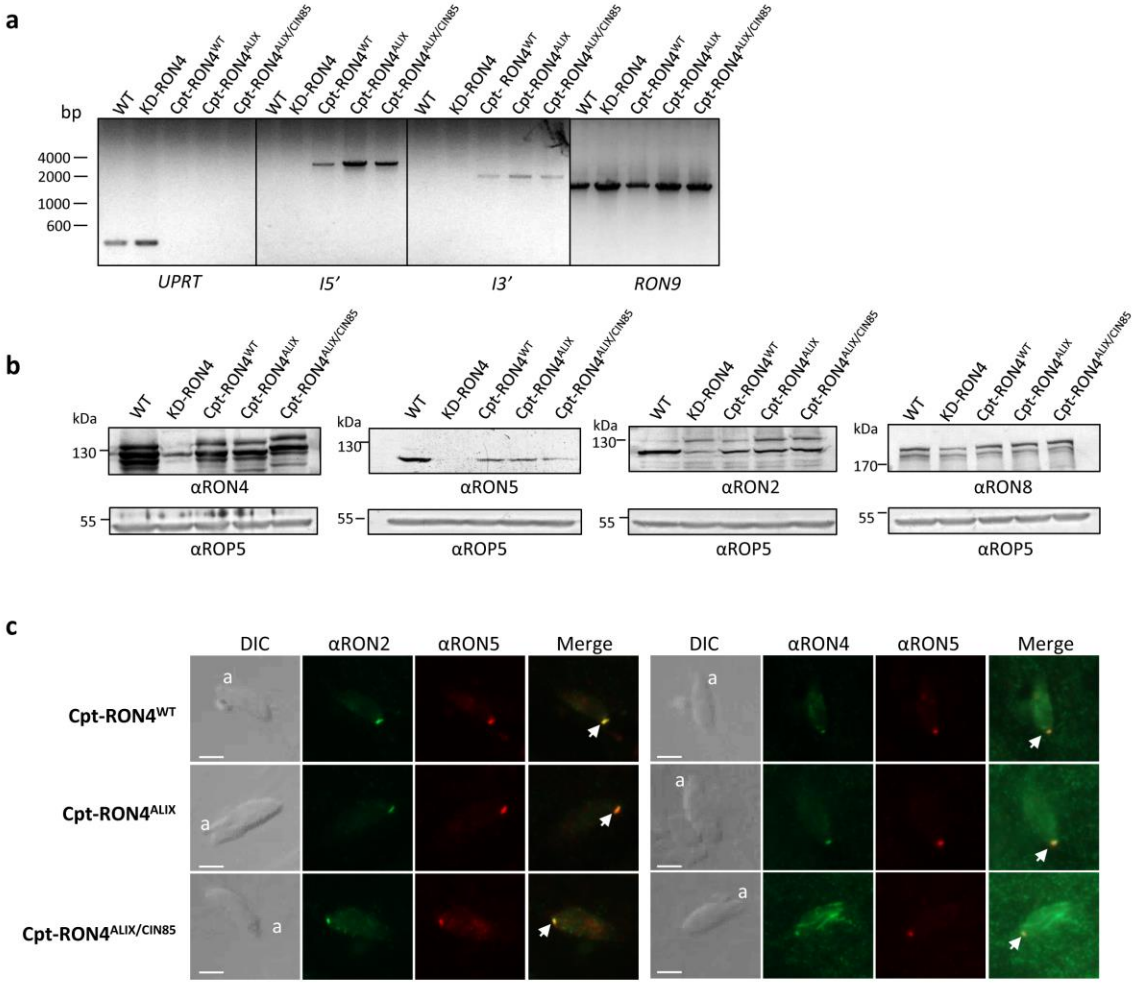

a, Complementation of KD-RON4 with a copy of RON4 mutated for both ALIX binding sites (YPNL into APNL: Cpt-RON4^{ALIX}) or for both ALIX binding sites and the three CIN85/CD2AP binding sites (Px[P/A]xPR to Ax[P/A]xA: Cpt-RON4$^{ALIX/CIN85}$) were verified by performing PCR *UPRT*, *I5'* and *I3'*,as described in Supplementary Fig. 4 for complementation with the wild-type copy of RON4. *RON9*: control PCR. **b,** Immunoblots of RON2, RON4, RON5 and RON8 proteins in WT, KD-RON4 and complemented strains treated for two days with ATc. Antibodies used are rabbit anti-RON2-3, rabbit anti-RON4,

rat anti-RON5N and rat-anti-RON8. For each RON, the expression levels are similar in Cpt-RON4^{WT}, Cpt-RON4^{ALIX} or Cpt-RON4$^{ALIX/CIN85}$ parasites. ROP5, loading control. **c,** IFAs of invading Cpt-RON4^{WT}, Cpt-RON4^{ALIX} and Cpt-RON4$^{ALIX/CIN85}$ parasites using rabbit anti-RON4, rabbit anti-RON2-4, rat anti-RON8 and rat anti-RON5N antibodies. Parasites were grown with ATc for two days. Scale bar, 2µm.

Supplementary Figure 6 | A functional ESCRT machinery is not present at the MJ.

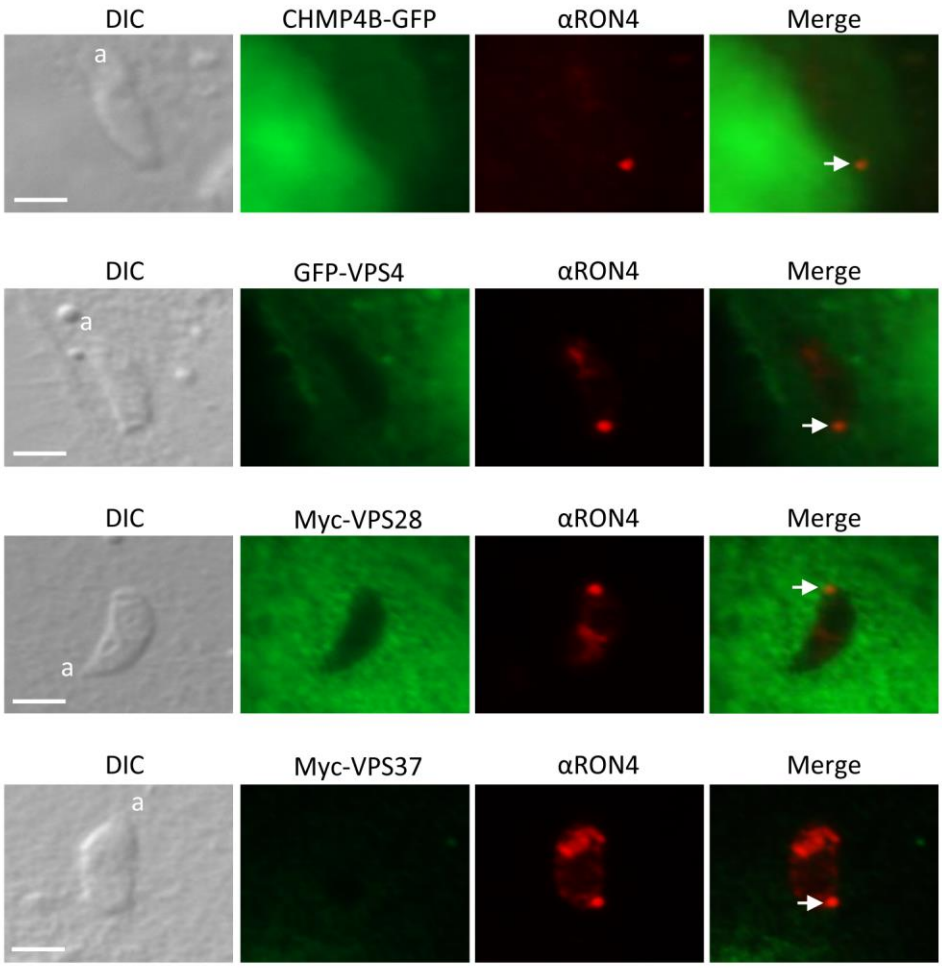

IFAs of invading *Δku80 TATi* parasites on HeLa cells transfected with plasmids allowing expression of CHMP4B-GFP, GFP-VPS4, myc-VPS28 or myc-VPS37. RON4 is stained with rabbit anti-RON4 antibodies. VPS28 and VPS37 are detected with anti-myc antibodies. CHMP4B and VPS4, two essential proteins of the ESCRT machinery, and VPS28 and VPS37, two members of the ESCRT-I sub-group, are not detected at the MJ. a, apical end; arrow, MJ. Scale bar, 2µm.

Supplementary Figure 7 | The P[T/S]AP motifs of RON5 are competent to bind TSG101 UEV.

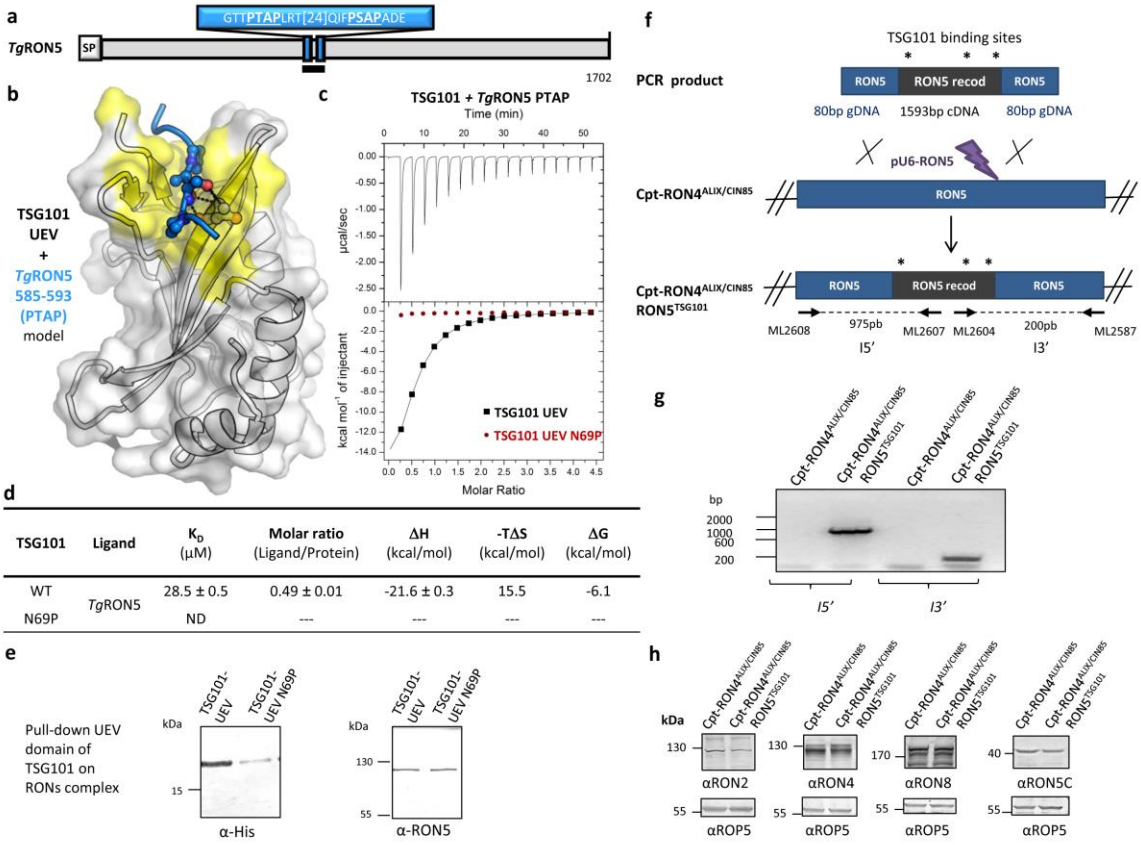

a, Schematic of the RON5 protein sequence, with the internal repeats of the P[T/S]AP motifs indicated by blue boxes. The black bar indicates the peptide used to investigate binding of RON5 to TSG101 UEV. SP, signal peptide. **b,** Semi-transparent surface of TSG101 UEV (white) bound to TgRON5 PTAP peptide (blue cartoon with the PTAP motif shown in sticks colored by element) (PDB ID 3OBU), with the interacting residues of TSG101 UEV colored yellow. Asn69 is shown as yellow sticks and was mutated (N69P) in this study as described previously[1]. **c,** Example ITC thermogram of TSG101 UEV WT and N69P interacting with RON5 PTAP GB1 at 20°C. **d,** Table of ITC results comparing binding affinities and thermodynamic profiles for the interaction of TSG101-UEV WT and

N69P with RON5 P[T/S]AP GB1 fusion at 20°C. Protein, sample in the ITC cell; Ligand, sample in syringe. RON5 can bind to TSG101 molecules. **e,** TSG101 binds to the RONs complex. The RON2/RON4/RON5/RON8 parasite complex was isolated on anti-RON2-4 coated beads, then the beads were incubated either with TSG101-UEV WT or TSG101-UEV N69P recombinant proteins. Blots were revealed with anti-His and anti-RON5N antibodies. **f,** Schematic representation of the strategy used to introduce point mutations of PPPY site into AAAA and P[T/S]AP sites into A[T/S]AA in the *RON5* gene in Cpt-RON4$^{ALIX/CIN85}$ parasites. Briefly, a 1593 bp PCR product of recodonized RON5 cDNA containing the desired mutations and flanked by 80 bp of genomic DNA (gDNA) is inserted into the RON5 locus in Cpt-RON4$^{ALIX/CIN85}$ parasites using the CRISPR/Cas9 strategy. The pU6-RON5 vector encodes for Cas9-YFP and a gRNA to induce a double break into the RON5 locus. YFP-positive clones were cloned using FACS sorting. **g,** PCR confirming the 5' and 3' integration of the PCR fragment. **h,** Immunoblots of RON proteins using rabbit anti-RON4, rabbit anti-RON2-3, rat anti-RON8, and rabbit anti-RON5C antibodies. Cpt-RON4$^{ALIX/CIN85}$ and Cpt-RON4$^{ALIX/CIN85}$/RON5^{TSG101} parasites expressed the same amount of each RON.

Supplementary Figure 8 | Mutations of ALIX binding sites at the endogenous *RON4* gene.

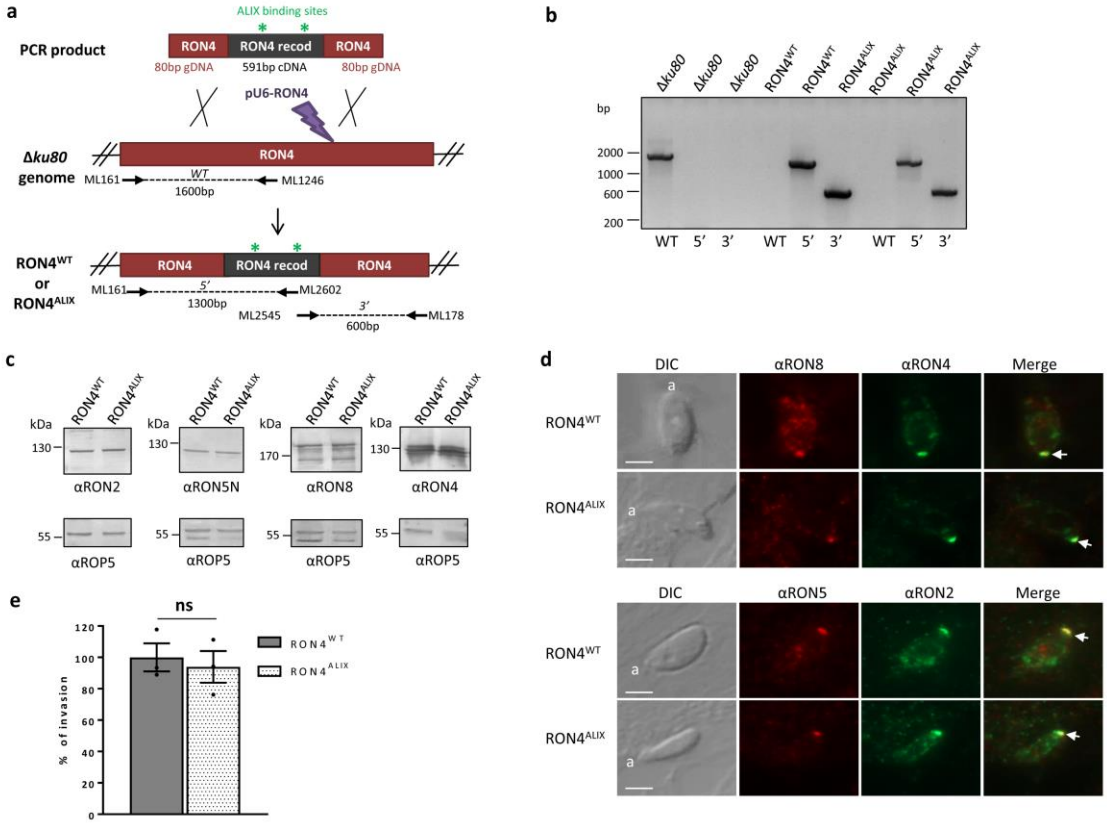

a, Schematic of the strategy used to introduce point mutations within *RON4* gene. The two YPNL motifs are changed into APNL. Briefly, a PCR product containing 591 bp of recodonized RON4 cDNA containing or not the desired mutations and flanked by 80 bp of genomic DNA (gDNA) is inserted into the *RON4* locus of *Δku80* parasite using the CRISPR/Cas9 strategy. The pU6-RON4 vector encodes for Cas9-YFP and a gRNA to induce a double break at the *RON4* locus. The resulting parasites contain a codon remodeled wild-type version of RON4 ($RON4^{WT}$) or a mutated version of RON4 for ALIX binding sites ($RON4^{ALIX}$). **b,** PCR products confirming the correct integration of codon remodeled WT or mutated version of RON4. **c,** Western blotting of $RON4^{WT}$ and

RON4^{ALIX} using rabbit anti-RON4, anti-RON2-3, rat anti-RON8 and rat anti-RON5N antibodies. ROP5, loading control. Both lines express comparable amounts of RON proteins. **d,** IFAs of invading RON4^{WT} and RON4^{ALIX} parasites on HFFs using rabbit anti-RON4, anti-RON2-4, rat anti-RON8 and rat anti-RON5N antibodies. a, apical end; arrow, MJ. Scale bar, 2µm. **e,** Invasion assay on HFFs cells for 1 hour of RON4^{WT} and RON4^{ALIX} parasites. Values represent means ± SD, n=3, from a representative experiment out of 3 independent assays. Student's *t*-test; ns: not significant.

Supplementary Figure 9 | Mutations of CIN85/CD2AP binding sites within the endogenous *RON4, RON5* and *RON2* genes.

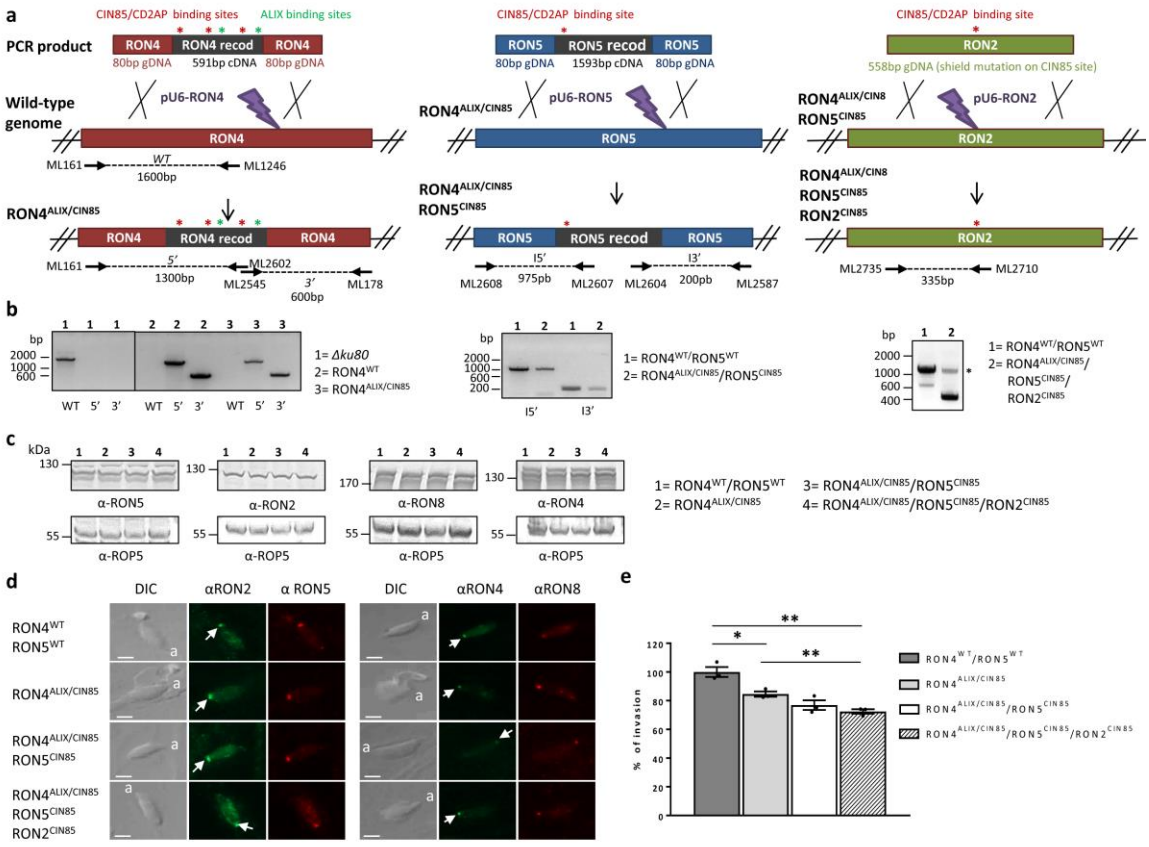

a, Schematics of the strategies used to introduce successive point mutations within the CIN85/CD2AP binding sites in RON4 (left), RON5 (middle) and RON2 (right) genes. The Px[P/A]xPR motifs are changed into Ax[P/A]xAA. Briefly, a PCR product containing 591 bp of recodonized RON4 cDNA with mutations for CIN85 and ALIX and flanked by 80 bp of RON4 genomic DNA (gDNA) is inserted into the RON4 locus of *Δku80* parasite using pU6-RON4 vector. The resulting parasites contain a mutated version of RON4 for ALIX and CIN85/CD2AP binding sites ($RON4^{ALIX/CIN85}$). For *RON5*, the donor DNA consists of a 1593 bp PCR product of recodonized *RON5* cDNA harbouring the mutation for CIN85 binding and flanked by 80 bp of genomic RON5 DNA. The replacement of the

endogenous DNA by the donor DNA in the *RON5* locus of RON4$^{ALIX/CIN85}$ parasite has been done using the CRISPR/Cas9 strategy and pU6-RON5 vector, yielding parasites named RON4$^{ALIX/CIN85}$/RON5^{CIN85}. Finally, to edit the *RON2* gene, a 558 bp PCR product of RON2 gDNA carrying the desired mutation Px[P/A]xPR to Px[P/A]xPA for CIN85 and a shield mutation in the PAM sequence was inserted in the *RON2* locus of RON4$^{ALIX/CIN85}$/RON5^{CIN85} parasite using CRISPR/Cas9 and pU6-RON2 vector. The resulting parasites are designated RON4$^{ALIX/CIN85}$/RON5^{CIN85}/RON2^{CIN85}. Parasites expressing recodonized WT versions of RON4 and RON5 have been generated (RON4^{WT}/RON5^{WT}) as control for c and d. **b,** PCRs confirming the correct integration of codon remodeled WT or mutated versions or RON4, RON5 and RON2. Primer ML2710 contains the mutation and hybridizes only to *RON2* mutated gene. The non-specific band is indicated by an asterisk. **c,** Western blotting of RON4^{WT}/RON5^{WT}, RON4$^{ALIX/CIN85}$, RON4$^{ALIX/CIN85}$/RON5^{CIN85} and RON4$^{ALIX/CIN85}$/RON5^{CIN85}/RON2^{CIN85} using rabbit anti-RON4, rabbit anti-RON2-3, rat anti-RON8 and rat anti-RON5N antibodies. ROP5, loading control. **d,** IFAs of invading RON4^{WT}/RON5^{WT}, RON4$^{ALIX/CIN85}$, RON4$^{ALIX/CIN85}$/RON5^{CIN85} and RON4$^{ALIX/CIN85}$/RON5^{CIN85}/RON2^{CIN85} on HFFs using rabbit anti-RON4, anti-RON2-4, rat anti-RON8 and rat anti-RON5N antibodies. a, apical end; arrow, MJ. Scale bar, 2µm. **e,** Invasion assay performed on HFF cells for 1 hour with RON4^{WT}/RON5^{WT}, RON4$^{ALIX/CIN85}$, RON4$^{ALIX/CIN85}$/RON5^{CIN85} and RON4$^{ALIX/CIN85}$/RON5^{CIN85}/RON2^{CIN85} parasites. Student's *t*-test; *p<0.05, **p<0.01; means ± s.e.m. for $n = 3$, from a representative experiment out of 2 independent assays.

.

Supplementary Figure 10 | Mutations of TSG101 binding sites in the endogenous *RON5* gene.

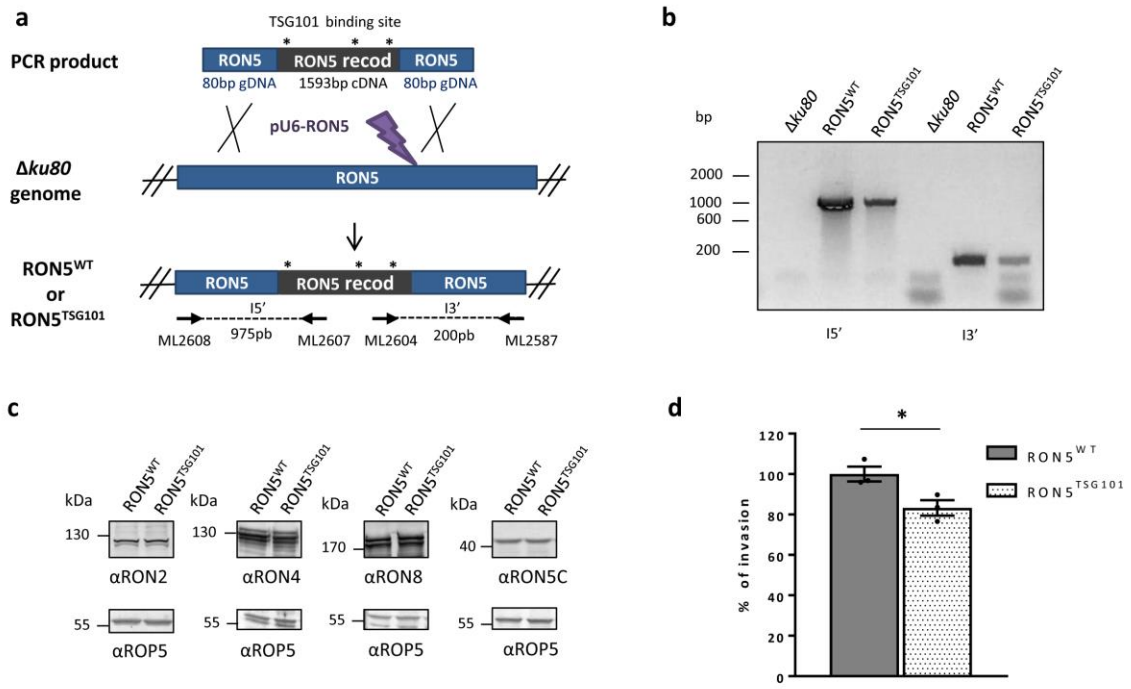

a, Schematic of the strategy used to introduce point mutations at *RON5* endogenous locus. The two P[T/S]AP motifs and the PPPY motif are changed into A[T/S]AA and AAAA. Briefly, a PCR product containing 1593 bp of recodonized RON5 cDNA containing or not the desired mutations and flanked by 80 bp of *RON5* genomic DNA is inserted into the *RON5* locus of *Δku80* parasite using the CRISPR/Cas9 strategy and pU6-RON5 vector. The resulting parasites contain a codon remodeled wild-type version of RON5 ($RON5^{WT}$) or a mutated version of RON5 for TSG101 binding sites ($RON5^{TSG101}$). **b,** PCR products confirming the correct integration of codon remodeled WT or mutated version of RON5. **c,** Western blotting of $RON5^{WT}$ and $RON5^{TSG101}$ using rabbit anti-RON4, rabbit anti-RON2-3, rat anti-RON8 and rat anti-RON5C antibodies. ROP5, loading control. **d,** Invasion assay on HFF cells for 1 hour of $RON5^{WT}$ and $RON5^{TSG101}$ parasites. Student's *t*-

test; *p<0.05; means ± s.e.m. for *n* = 3, from a representative experiment out of 2 independent assays.

Supplementary Figure 11 │ Full blots of results

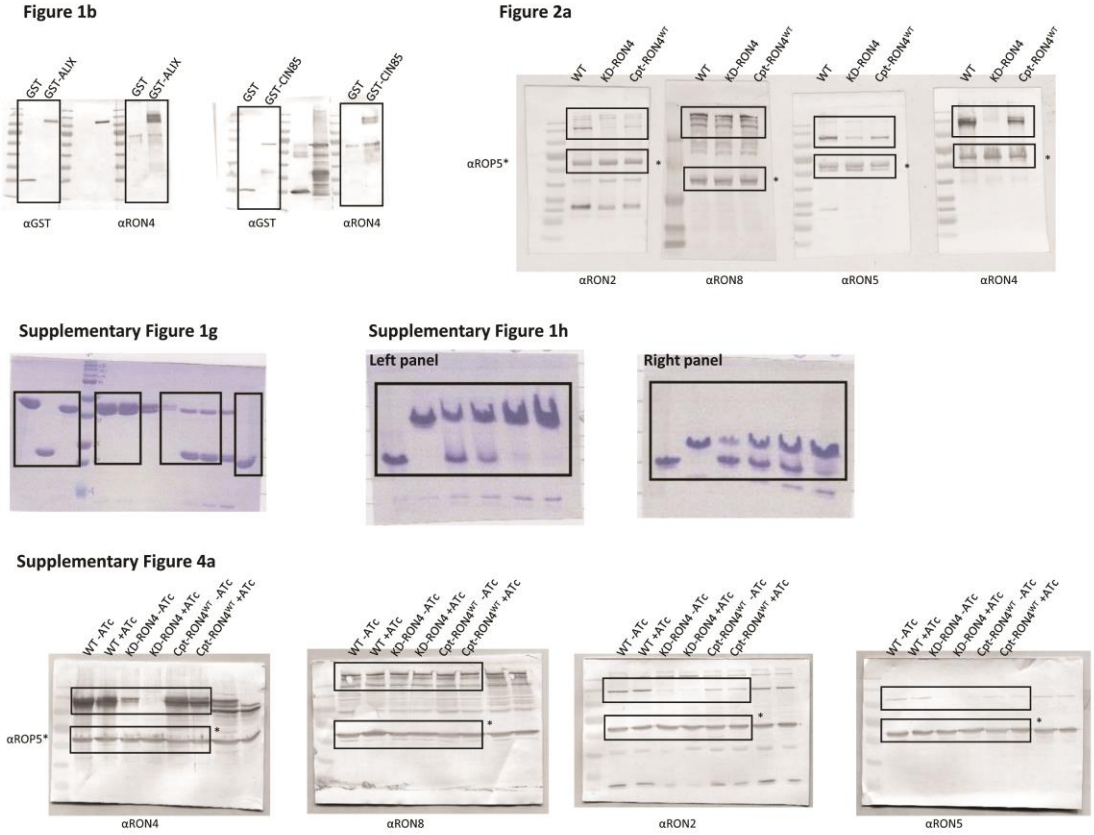

Full blots of results (continued)

Supplementary Figure 4d

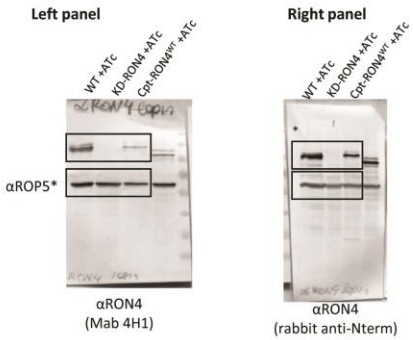

Supplementary Figure 5b

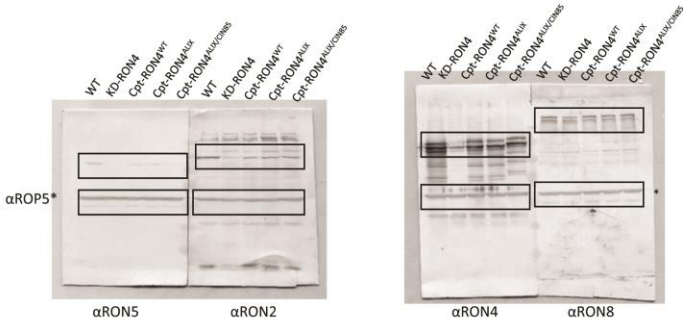

Supplementary Figure 7e

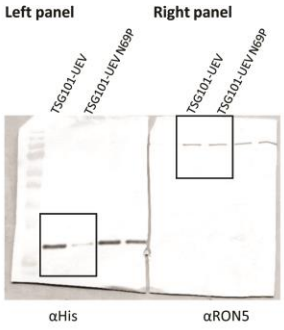

Supplementary Figure 7h

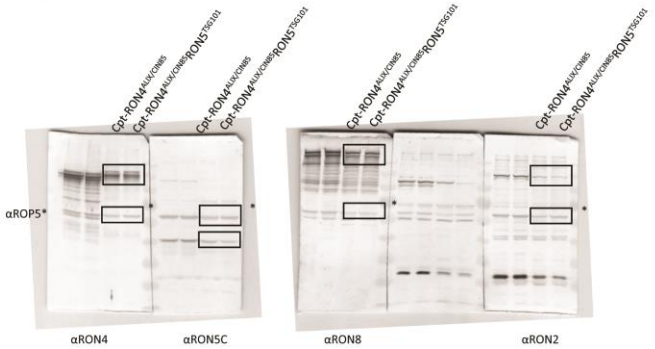

Full blots of results (continued)

Supplementary Figure 8c

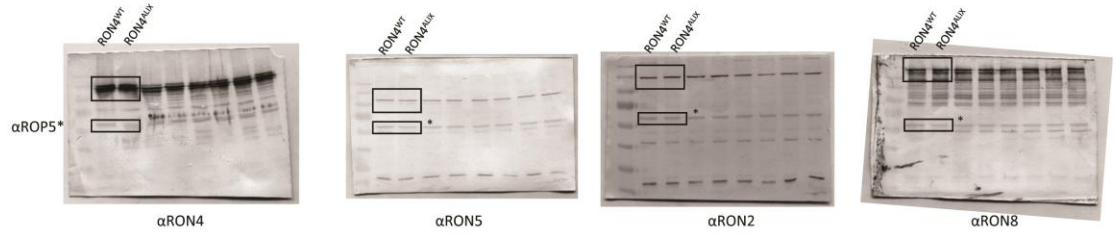

Supplementary Figure 9c

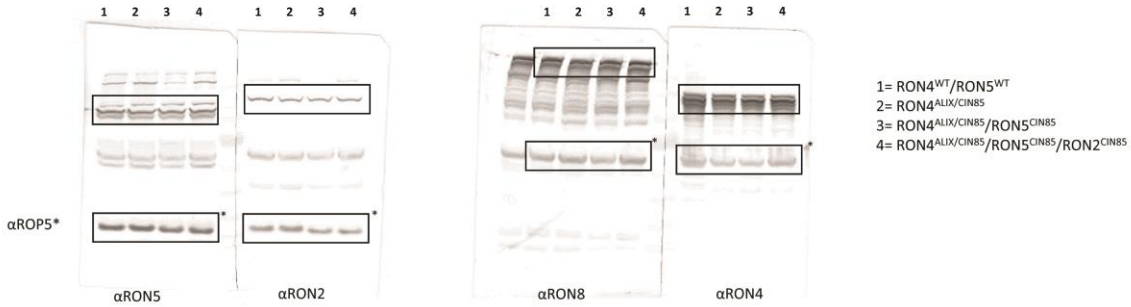

Supplementary Figure 10c

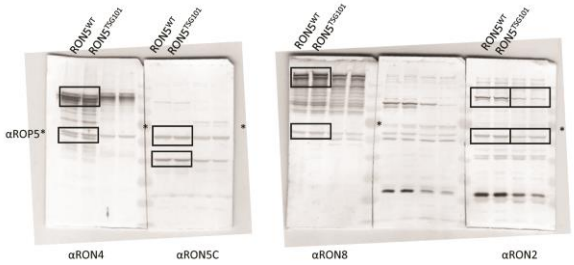

Supplementary Table 1. Yeast-Two hybrid with RON4 as a bait

Prey Name	Start…Stop (nt)	Number of clones
ALIX	..2256	1
ALIX	759-2240	1
ALIX	1047-2226	3
ALIX	1080-2256	14
ALIX	1080…	1
ALIX	1083-2241	3
ALIX	1124-2243	2
ALIX	1125-2256	2
ALIX	1131-2178	9
ALIX	1215-2235	9
ALIX	1230-2220	8
ALIX	1230…	2
CIN85	612-933	2

Supplementary Table 2. Primers used (excel document)

Supplementary Table 3. Antibodies used.

Antibody	Species	WB dilution	IFA dilution	Reference
Anti-RON4	Rabbit	1/1000e	1/1000[e]	[2]
Anti-SAG1	Mouse T41E5	-	1/2000[e]	[3]

Anti-SAG1	Rabbit	-	1/1000e	[4]
Anti-ROP1	Rabbit	-	1/1000e	[5]
Anti-RON4	Mouse T54H1	-	undiluted hybridoma	[6]
Anti-ROP5	Mouse T53E2	1/0000e	-	[7]
Anti-RON2-4	Rabbit	-	1/1000e	[2]
Anti-RON2-3	Rabbit	1/1000e	-	[2]
Anti-RON5N	Rat	1/500e	1/200e	[2]
Anti-RON5C	Rabbit	1/200e	-	[8]
Anti-RON8	Rat	1/500e	1/200e	[2]
Anti-RON4N	Rabbit	1/200e	1/1000e	[2]
Anti-ALIX	Mouse	1/500e	1/200e	SantaCruz sc-5354
Anti-GST	Rat	1/500e	1/200e	[9]
Anti-His	Mouse	1/3000e	-	Sigma H1029
Anti-Myc	Mouse	-	1/200e	SantaCruz sc-40

Supplementary Text

RON4 depletion induced improper targeting of RON2 and RON5 and a defect of invasion

A conditional RON4 knock-down was generated in *Δku80 TATi* strain by replacing the endogenous promoter by an ATc repressible promoter (Supplementary Fig. 3a) as described previously[10]. This mutant (named hereafter KD-RON4 for knock-down RON4) was selected with a DFHR selectable marker. Correct integration of the pKD-RON4 plasmid in the KD-RON4 strain was verified by PCR amplifications (Supplementary Fig. 3b) and sequencing. To complement KD-RON4 parasites, an additional copy of RON4 under 2kb of the 5' non coding region of *RON4* gene was inserted at the UPRT locus using the FUDR negative selection[10] (Supplementary Fig. 3c). In order to increase integration efficiency, a CRISPR/Cas9 strategy targeting the UPRT locus was used. PCR amplifications and sequencing were used to verify the correct integration (Supplementary Fig. 3d).

Without addition of ATc (to repress RON4 transcription), the expression of RON4 protein decreases in the KD-RON4 mutant as observed by western blot using a rabbit polyclonal antibody (Supplementary Fig. 4a) and RON4 was not detectable in the neck of the rhoptries (Supplementary Fig. 4b), indicating that expression from ATc repressible promoter dramatically reduces RON4 expression, as already published for a conditional KD-RON2 mutant[5] and to a lower extent for a KD-RON5 mutant[8]. After two days ATc treatment, the protein becomes almost undetectable by western blot or IFA (Supplementary Fig. 4a,b). RON4 was not detectable at the MJ of KD-RON4 parasites, even in absence of ATc (Supplementary Fig. 4c). Western blot analysis showed that RON4 expression in the

complemented strain (Cpt-RON4^{WT}) was much lower compared to wild-type, although it was driven by 2 kb of the 5' non coding region of *RON4* (Supplementary Fig. 4a). Partial restoration (less than 60%) is confirmed using two additional RON4 antibodies (Supplementary Fig. 4d).

As observed for KD-RON2[5] and KD-RON5[8] parasites, RON8 is expressed normally (Supplementary Fig. 4a) and is correctly localized at the rhoptries (Supplementary Fig. 4b) and at the MJ (Supplementary Fig. 4c) during invasion. In contrast, the expression of RON2 and RON5 decreases dramatically in the KD-RON4 mutant (Supplementary Fig. 4a). The addition of ATc did not accentuate the depletion. RON2 and RON5 proteins partially localize to the neck of the rhoptries in intracellular parasites (Supplementary Fig. 4b) and are almost undetectable at the MJ in invading parasites (Supplementary Fig. 4c). In agreement with the co-expression of both RON2 and RON5 with RON4, RON2 and RON5 expression are also partially restored in the complemented strain (Supplementary Fig. 4a). IFA on intracellular (Supplementary Fig. 4b) and invading (Supplementary Fig. 4c) parasites confirm the re-expression of RON4, RON2 and RON5 in the neck of the rhoptry and at the MJ.

Thus, it is clear that RON4 is required for proper formation of the RON2/RON4/RON5 complex, and the phenotypes associated with the RON4 knock-down cell line *in vitro* described in the main text are actually due to knock-down of RON2, RON4 and RON5 proteins.

The KD-RON4 parasite does not present any replication defect (Supplementary Fig. 5e) but show a substantial reduction in invasion rate (Supplementary Fig. 4f). Invasion is inhibited by 50% in absence of ATc compared to the parental strain, and up to 60% when

strains have been treated with ATc for two days. This defect was somewhat moderate when compared to the strong inhibition of invasion in KD-RON2 (up to 80%)[5]. This was likely due to residual expression of RON2 and RON5 in the neck of the rhoptries in the KD-RON4 parasites and the faint signal of those proteins at the MJ in some parasites. In contrast, in KD-RON2, both RON4 and RON5 are totally mistargeted [5]. The decrease of invasion in cKD-RON4 was reversed (approximately 80%) but never reached the normal invasion rate, a result, which might be easily explained by the incomplete restoration of the expression of RONs (Supplementary Fig. 4a). Collectively, these data show that RON4 is important for proper expression of RON2 and RON4 and that the KD-RON4 parasite displays reduced invasion *in vitro* specifically due to decrease of RON2, RON4 and RON5 expression.

Supplementary References

1 Im, Y. J. *et al.* Crystallographic and functional analysis of the ESCRT-I /HIV-1 Gag PTAP interaction. *Structure* **18**, 1536-1547, doi:10.1016/j.str.2010.08.010 (2010).

2 Besteiro, S., Michelin, A., Poncet, J., Dubremetz, J. F. & Lebrun, M. Export of a *Toxoplasma gondii* rhoptry neck protein complex at the host cell membrane to form the moving junction during invasion. *PLoS Pathog* **5**, e1000309 (2009).

3 Couvreur, G., Sadak, A., Fortier, B. & Dubremetz, J. F. Surface antigens of Toxoplasma gondii. *Parasitology* **97 (Pt 1)**, 1-10 (1988).

4 Harning, D., Spenter, J., Metsis, A., Vuust, J. & Petersen, E. Recombinant Toxoplasma gondii surface antigen 1 (P30) expressed in Escherichia coli is recognized by human *Toxoplasma*-specific immunoglobulin M (IgM) and IgG antibodies. *Clinical and diagnostic laboratory immunology* **3**, 355-357 (1996).

5 Lamarque, M. H. *et al.* Plasticity and redundancy among AMA-RON pairs ensure host cell entry of *Toxoplasma* parasites. *Nat Commun* **5**, 4098, doi:10.1038/ncomms5098 (2014).

6 Lebrun, M. *et al.* The rhoptry neck protein RON4 relocalizes at the moving junction during *Toxoplasma gondi*i invasion. *Cell Microbiol* **7**, 1823-1833 (2005).

7 Leriche, M. A. & Dubremetz, J. F. Characterization of the protein contents of rhoptries and dense granules of *Toxoplasma gondii* tachyzoites by subcellular fractionation and monoclonal antibodies. *Mol Biochem Parasitol* **45**, 249-259 (1991).

8 Beck, J. R., Chen, A. L., Kim, E. W. & Bradley, P. J. RON5 is critical for organization and function of the Toxoplasma moving junction complex. *PLoS Pathog* **10**, e1004025, doi:10.1371/journal.ppat.1004025 (2014).

9 Lamarque, M. *et al.* The RON2-AMA1 interaction is a critical step in moving junction-dependent invasion by apicomplexan parasites. *PLoS Pathog* **7**, e1001276 (2011).

10 Sheiner, L. *et al.* A systematic screen to discover and analyze apicoplast proteins identifies a conserved and essential protein import factor. *PLoS Pathog* **7**, e1002392, doi:10.1371/journal.ppat.1002392 (2011).